STRUCTURAL BIOLOGY COMMUNICATIONS

ISSN 2053-230X

Crystal structure of monomeric Amuc_1100 from *Akkermansia muciniphila*

Luqiu Mou,[a] Xi Peng,[a] Yan Chen,[b,c] Qingjie Xiao,[a] Huijuan Liao,[b,c] Mingfeng Liu,[b,c] Li Guo,[a] Yang Liu,[c,d] Xiaohu Zhang[b,c]* and Dong Deng[a]*

[a]Division of Obstetrics, Key Laboratory of Birth Defects and Related Diseases of Women and Children of MOE, State Key Laboratory of Biotherapy, West China Second Hospital, Sichuan University, Chengdu, Sichuan 610041, People's Republic of China, [b]Sichuan University–The Chinese University of Hong Kong Joint Laboratory for Reproductive Medicine, West China Second University Hospital, Sichuan University, Chengdu, Sichuan 610041, People's Republic of China, [c]Key Laboratory of Birth Defects and Related Diseases of Women and Children (Sichuan University), Ministry of Education, West China Second University Hospital, Sichuan University, Chengdu, Sichuan 610041, People's Republic of China, and [d]Department of Pediatrics, West China Second University Hospital, Sichuan University, Chengdu, Sichuan 610041, People's Republic of China. *Correspondence e-mail: zhangxh_alex@163.com, dengd@scu.edu.cn

Received 15 January 2020
Accepted 24 March 2020

Edited by F. T. Tsai, Baylor College of Medicine, Houston, USA

Keywords: *Akkermansia muciniphila*; type IV pili; Amuc_1100; gut microbes; crystal structure.

PDB reference: Amuc_1100 from *Akkermansia muciniphila*, 6kny

Supporting information: this article has supporting information at journals.iucr.org/f

Many human diseases, such as obesity and diabetes, show annual increases in prevalence and often involve intestinal microbes. One such probiotic bacterium, *Akkermansia muciniphila*, which was discovered a decade ago, has been reported to influence glucose homeostasis and to contribute to gut health. Amuc_1100, a functionally uncharacterized protein of *A. muciniphila*, was found to be a key active component in reducing the body weight of mice. Here, the crystal structure of Amuc_1100 (residues 31–317), referred to as Amuc_1100*, is reported at 2.1 Å resolution. Amuc_1100* has a similar fold to three proteins related to pilus formation, PilO, PilN and EpsL, indicating a similar function. Biochemical investigations further confirmed a monomeric state for the soluble region of Amuc_1100, which differs from the dimeric states of PilO, PilN and EpsL. This study provides a structural basis for the elucidation of the molecular mechanism of Amuc_1100.

1. Introduction

The gut microbiota is a complex community that plays essential roles in host nutrition, metabolism and immunity regulation (Li *et al.*, 2011; Everard *et al.*, 2013). The varied constituents and/or functions of gut microbes are related to many chronic diseases, including colon cancer, colitis (Vigsnaes *et al.*, 2012), irritable bowel syndrome (Png *et al.*, 2010), obesity and diabetes (Clemente *et al.*, 2012). A study has demonstrated that intestinal bacteria affect the physiology of the host by secreting various metabolites or bacterial products (Li *et al.*, 2016). Many researchers have noted that the constituents of probiotic bacteria have an important function in human health.

One such probiotic bacterium, *Akkermansia muciniphila*, which was discovered a decade ago (Collado *et al.*, 2007; Derrien *et al.*, 2008), has been shown to improve glucose homeostasis and to contribute to gut health (Everard *et al.*, 2013; Dao *et al.*, 2016). *A. muciniphila* is an anaerobic, Gram-negative bacterium covered by a mucosal layer that resides in the human intestinal tract (Ottman *et al.*, 2016). Its growth is sustained by mucin degradation, and this bacterium produces diverse metabolites such as short-chain fatty acids (SCFAs) and other byproducts to promote the growth of other probiotics (Shen *et al.*, 2017). *A. muciniphila* attaches to intestinal cells and strengthens the integrity of the epithelial

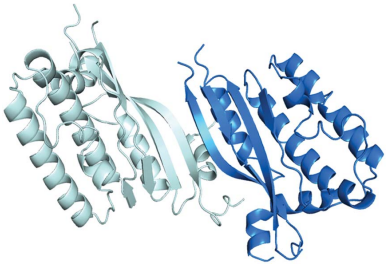

layer. When cocultured with epithelial cell lines such as Caco-2 and HT-29, *A. muciniphila* increased their monolayer integrity and transepithelial electric resistance (Reunanen *et al.*, 2015). A higher relative abundance of *A. muciniphila* is correlated with a healthy metabolic state in overweight and obese humans. Oral administration of *A. muciniphila* increased mucin layer thickness, decreased endotoxemia and increased the number of goblet cells (Dao *et al.*, 2016). This evidence prompted researchers to further investigate the mechanisms by which *A. muciniphila* provides these benefits.

Recently, studies of the bacterial genome and proteome identified an outer membrane protein in *A. muciniphila*, Amuc_1100, which improved glucose tolerance in mice after oral administration of the purified protein (Cani & de Vos, 2017; Plovier *et al.*, 2017; Ottman *et al.*, 2017). Notably, electron-microscopy studies have shown that *A. muciniphila* has a type IV pilus-like structure (Derrien *et al.*, 2004). In Gram-negative bacteria, type IV pili (T4P) have various important functions in bacterial pathogenicity, including host attachment, biofilm formation and twitching motility (Bahar *et al.*, 2009). T4P interact with host cells and thus induce immune responses in the host (Craig *et al.*, 2004). Interestingly, the presence of Amuc_1100 within a gene cluster involved in type IV pilus-like formation indicates that its role is related to the formation of a pilus-like structure (Ottman *et al.*, 2016). Amuc_1100 may play an important role in the interplay between microbes and hosts. However, Amuc_1100 does not share sequence similarity with other proteins involved in type IV pili formation.

Here, we report the crystal structure of Amuc_1100 (residues 31–317; referred to as Amuc_1100*) at 2.1 Å resolution. A comparison with known structures indicated a similar function for Amuc_1100 and PilO (Sampaleanu *et al.*, 2009), an inner membrane protein that is essential for T4P biogenesis in *Pseudomonas aeruginosa*. PilO proteins are components of the alignment subcomplex of T4P and form homodimers *in vivo* (Leighton *et al.*, 2016). However, both the biochemical and structural investigations in this study suggested that Amuc_1100* is a monomer. Structural investigation of Amuc_1100 will shed light on the therapeutic mechanism of this bacterium as well as the formation of T4P in *A. muciniphila.*

2. Materials and methods

2.1. Macromolecule production

Codon-optimized cDNA for the full-length Amuc_1100 protein (NCBI accession No. WP_012420141.1) was synthesized by Qinglan Biotech, People's Republic of China. The truncated construct for Amuc_1100 (residues 31–317), named Amuc_1100*, was subcloned into a modified pET-15b vector with an N-terminal 6×His tag followed by a drICE cutting site. Amuc_1100* was expressed in *Escherichia coli* BL21 (DE3) cells using Luria–Bertani medium (10 g l^{-1} tryptone, 10 g l^{-1} NaCl, 5 g l^{-1} yeast extract) in a shaker (220 rev min^{-1}) at 310 K. When the cell density reached an OD_{600} of 1.0, 0.2 m*M* isopropyl β-D-1-thiogalactopyranoside (IPTG) was added to induce protein expression at 291 K for 12 h. The cells were harvested and resuspended in lysis buffer consisting of 25 m*M* Tris pH 8.0, 150 m*M* NaCl, 1 m*M* phenylmethylsulfonyl fluoride (PMSF; Aladdin) and disrupted using sonication. After centrifugation at 50 000*g* for 45 min, the supernatant was loaded onto a prepackaged Ni–NTA column for affinity purification. The resin was rinsed with wash buffer consisting of 25 m*M* Tris pH 8.0, 150 m*M* NaCl, 15 m*M* imidazole and was eluted with elution buffer (wash buffer plus 300 m*M* imidazole). The affinity-purified protein was diluted with buffer *A* [25 m*M* Tris pH 8.0, 5 m*M* dithiothreitol (DTT)] and further purified using an ion-exchange column (Source 15Q, GE Healthcare). The peak fractions were collected and concentrated for drICE digestion. After the removal of the tag, the protein was subjected to gel-filtration chromatography (Superdex 200 Increase 10/300 GL, GE Healthcare) in buffer consisting of 25 m*M* Tris pH 8.0, 150 m*M* NaCl, 5 m*M* DTT. To determine the protein concentration, the UV absorbance of Amuc_1100 at 280 nm was measured. The protein concentration was calculated from the UV absorbance using a molar extinction coefficient of 0.65. The peak fractions were concentrated to 20 mg ml^{-1} for crystallization. Other truncations of Amuc_1100 were expressed and purified using an identical protocol. Information related to the production of Amuc_1100* is summarized in Table 1.

Table 1
Macromolecule-production information.

Source organism	*A. muciniphila* (strain ATCC BAA-835/Muc)
DNA source	Synthesized
Forward primer	GATGAAGTTGATGCACATATGATTGTGAATAGCAAACGC
Reverse primer	GTTAGCAGCCGGATCCTTCTCGAGTCATTAATCTTCGCTCGGTTCCTG
Cloning vector	Modified pET-15b
Expression vector	Modified pET-15b
Expression host	*E. coli* BL21 (DE3)
Complete amino-acid sequence of the construct produced	MGSSHHHHHHSSGLVPRGSHSDEVDAHMIVNSKRSELDKKISIAAKEIKSANAAEITPSRSSNEELEKELNRYAKAVGSLETAYKPFLASSALVPTTPTAFQNELKTFRDSLISSCKKKNILITDTSSWLGFQVYSTQAPSVQAASTLGFELKAINSLVNKLAECGLSKFIKVYRPQLPIETPANNPEESDEADQAPWTPMPLEIAFQGDRESVLKAMNAITGMQDYLFTVNSIRIRNERMMPPPIANPAAAKPAAAQPATGAASLTPADEAAAPAAPAIQQVIKPYMGKEQVFVQVSLNLVHFNQPKAQEPSED

2.2. Crystallization

The crystallization of several Amuc_1100 truncations was attempted. Only Amuc_1100* that had been treated with 0.01 mg ml^{-1} trypsin before establishing the crystallization trials gave reasonable diffraction data. The crystals of Amuc_1100* were grown at 291 K by the sitting-drop vapor-diffusion method in buffer consisting of 0.2 *M* K_2HPO_4, 1.8 *M* NaH_2PO_4, 0.1 *M* Na_2HPO_4/citric acid pH 4.2. Triangle-shaped crystals grew to full size over 20 d. Bromide-derived crystals were obtained by soaking in the mother liquor plus 0.3 *M*

Table 2
Crystallization.

Method	Vapor diffusion, sitting drop
Plate type	48-well double-sample sitting-drop crystallization plate
Temperature (K)	291
Protein concentration (mg ml^{-1})	20
Buffer composition of protein solution	25 m*M* Tris pH 8.0, 150 m*M* NaCl, 5 m*M* DTT
Composition of reservoir solution	0.2 *M* K_2HPO_4, 1.8 *M* NaH_2PO_4, 0.1 *M* Na_2HPO_4/citric acid pH 4.2
Volume and ratio of drop	2 µl drop, 1:1 ratio
Volume of reservoir (µl)	70

Table 3
Data collection and processing.

Data	Native	Br (peak)
Diffraction source	BL19U1, SSRF	BL19U1, SSRF
Wavelength (Å)	0.9793	0.9190
Temperature (K)	100	100
Detector	PILATUS3 6M	PILATUS3 6M
Crystal-to-detector distance (mm)	350	400
Rotation range per image (°)	1	1
Total rotation range (°)	180	1800
Exposure time per image (s)	0.3	0.15
Space group	$C222_1$	$C222_1$
a, *b*, *c* (Å)	77.5, 119.8, 97.4	79.3, 119.2, 97.6
α, β, γ (°)	90, 90, 90	90, 90, 90
Mosaicity (°)	0.4	0.6
Resolution range (Å)	40–2.1 (2.18–2.10)	30–2.6 (2.69–2.60)
Total No. of reflections	173489	937292
No. of unique reflections	26899 (2620)	14601 (1437)
Completeness (%)	100 (99.7)	100 (100)
Multiplicity	6.4 (5.8)	64.2 (58.5)
$\langle I/\sigma(I)\rangle$	11.7 (1.6)	25.0 (6.0)
$CC_{1/2}$	0.98 (0.73)	0.99 (0.98)
$R_{r.i.m.}$	0.15 (0.92)	0.18 (0.71)
$R_{p.i.m.}$	0.06 (0.38)	0.02 (0.10)
Overall *B* factor from Wilson plot (Å^2)	27.74	29.32

NaBr and 30% glycerol for 1 h. Crystallization information is summarized in Table 2.

2.3. Data collection and processing

Diffraction data sets for native and bromide-derived crystals were collected on beamline BL19U1 at Shanghai Synchrotron Radiation Facility (SSRF). All data sets were processed with the *HKL*-3000 package (Minor *et al.*, 2006). Further processing was performed using the *CCP*4 suite (Winn *et al.*, 2011). Data-collection and processing statistics are summarized in Table 3.

2.4. Structure solution and refinement

The initial phasing and crude model of Amuc_1100* were obtained from bromide-based single anomalous diffraction (SAD) data using *CRANK*2 in the *CCP*4 suite (Winn *et al.*, 2011). The structure of Amuc_1100* was solved by molecular replacement with the bromide-derived crude model as the search model using *Phaser* (McCoy *et al.*, 2007). The structure was further refined with *Coot* (Emsley *et al.*, 2010) and *Phenix* (Liebschner *et al.*, 2019). Structure-solution and refinement statistics are summarized in Table 4.

Table 4
Structure refinement.

Resolution range (Å)	39–2.1 (2.17–2.10)
Completeness (%)	99.9
σ Cutoff	$F > 1.370\sigma(F)$
No. of reflections, working set	24872 (2303)
No. of reflections, test set	1998 (185)
Final R_{cryst}	0.19 (0.26)
Final R_{free}	0.21 (0.28)
No. of non-H atoms	
Total	2993
Protein	2824
Ligand	0
Water	169
Total	2993
R.m.s. deviations	
Bonds (Å)	0.01
Angles (°)	0.26
Average *B* factors (Å^2)	
Overall	34.77
Protein	34.3
Water	43.2
Ramachandran plot	
Most favored (%)	99.43
Allowed (%)	0.57

3. Results and discussion

3.1. Characterization of monomeric Amuc_1100*

We purified the truncated Amuc_1100 (residues 31–317; named Amuc_1100*), which lacks the predicted N-terminal transmembrane region and was used for oral administration in a previous study (Plovier *et al.*, 2017), for structural investigation (Fig. 1*a* and Supplementary Fig. S1*a*). As shown by size-exclusion chromatography, Amuc_1100* exists in a monomeric state in solution (Supplementary Fig. S1*a*). This result is consistent with the theoretical molecular weight (31.2 kDa) of Amuc_1100*. To further confirm the monomeric state of Amuc_1100*, we performed analytical ultracentrifugation (AUC; Fig. 1*b*) and static light scattering (SLS; Fig. 1*c*).

Various truncated proteins (Supplementary Fig. S1*b*) were also purified for crystal screening. Of these, all N-terminally truncated proteins presented monodisperse behavior similar to that of Amuc_1100*, whereas C-terminal truncations (residues 31–292, 31–300 or 31–310) displayed either aggregation or undetectable expression (Supplementary Fig. S1*b*).

3.2. Crystal structure of Amuc_1100*

Systematic crystallization trials were carried out with the N-terminal truncations, and crystals with various shapes grew under different conditions (Supplementary Fig. S1*c*). However, the diffraction data from all of the crystals were not suitable for solving the structure of Amuc_1100. Limited proteolysis was thus introduced to remove the flexible region of Amuc_1100* for crystallization. A previous study showed that oral administration of the purified Amuc_1100* protein could improve metabolism in diabetic mice (Plovier *et al.*,

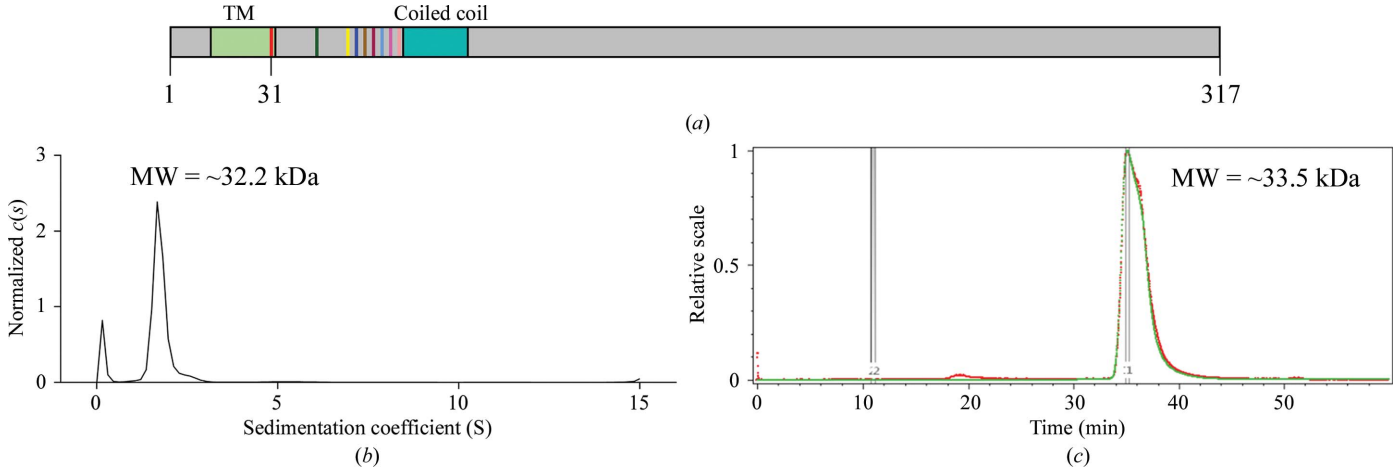

Figure 1
Characterization of Amuc_1100*. (*a*) Predicted diagram of Amuc_1100. The transmembrane region (TM) and coiled-coil domain are colored light green and cyan, respectively. Residues 31–317 are the protein construct used in this experiment. Different truncated versions are indicated in various colors. (*b*) Analytical ultracentrifugation (AUC) analysis of Amuc_1100*. The horizontal axis is the sedimentation coefficient and the vertical axis is the normalized $c(s)$. The molecular weight of Amuc_1100* is approximately 32.2 kDa. (*c*) Static light-scattering (SLS) results. The horizontal axis represents time and the vertical axis represents the relative scale. The molecular weight of Amuc_1100* is approximately 33.5 kDa.

2017), indicating that Amuc_1100* may be digested by proteases, such as trypsin, in the digestive tract. Therefore, we crystallized Amuc_1100 by adding 0.01 mg ml^{-1} trypsin and collected a diffraction data set from the triangular-shaped crystals (Supplementary Figs. S2*a*–S2*c*). Using single anomalous diffraction (SAD; Rice *et al.*, 2000), we solved and refined the structure of Amuc_1100* at 2.1 Å resolution (Tables 3 and 4).

In the asymmetric unit, there are two Amuc_1100* molecules packed in an antiparallel pattern with an approximately 70° angle (Fig. 2*a*). Superposition of the two molecules showed a root-mean-square deviation (r.m.s.d.) of approximately 0.4 Å over 136 C^{α} atoms, suggesting a consistent conformation of the two molecules (Fig. 2*b*). The overall structure of Amuc_1100* contains six α-helices and four β-sheets that form a bouquet (Fig. 2*c*). The N-terminal α1 helix connects helices α2, α3 and α4, while β1, which is near α3 and α4, connects α4 to α5, and the antiparallel β-sheets β2–β4 are associated with α6. Internal flexible regions are responsible for all connections (Fig. 2*c*).

The well defined regions of trypsin-cleaved Amuc_1100* consist of three fragments, residues 79–184, 196–242 and 292–311 (Fig. 2), while some fragments are missing. We further harvested numerous crystals to analyze the accurate boundaries of the crystallized Amuc_1100 using SDS–PAGE, in which an approximately 28 kDa major band was detected (Supplementary Fig. S2*e*). This finding suggests that the major cleavage events are located near the N-terminus or the C-terminus. As shown by further N-terminal sequencing of the crystallized Amuc_1100, the first residue at the N-terminus was an alanine, followed by valine, glycine, serine and leucine (Supplementary Fig. S2*e*). Considering that trypsin-cleaved peptides theoretically end at the carboxyl side group of an arginine or lysine residue, we confirmed that the crystallized Amuc_1100 was cleaved at the carboxyl end of Lys77. Because there were no lysines or arginines after the visible residue Ala311 in the structure, the boundaries of crystallized Amuc_1100 should be 78–317.

3.3. Structural analyses for functional implications

In previous studies, Amuc_1100 was defined as a pilus-like protein involved in pilus assembly (Ottman *et al.*, 2016, 2017). However, sequence alignments between Amuc_1100 and proteins related to pilus formation (PilC, PilD, PilE, PilF, PilG, PilH, PilI, PilJ, PilL, PilK, PilM, PilN, PilO, PilP, PilQ and PilW) presented similarities lower than 20%. Therefore, we tried to understand the function at the structural level and compared the structure of Amuc_1100* with known structures in the Protein Data Bank using *DALI* (Holm & Sander, 1995). Interestingly, we found that Amuc_1100* shares a similar fold with two piliation-related proteins, PilN and PilO, and proteins related to the type 2 secretion system (T2SS) such as EpsL (Fig. 3). The *Z*-scores obtained from *DALI* are 6.0, 9.6 and 6.5, respectively. The r.m.s.d. values are 3.1, 3.0 and 2.3 Å for PilN, PilO and EpsL, respectively. Surprisingly, PilN, PilO and EpsL are dimers, whereas Amuc_1100* is a monomer (Figs. 3*d*–3*f*). To compare the interfaces in these structures, we explored the interface between two Amuc_1100 molecules in the asymmetric unit using *PISA* (https://www.ebi.ac.uk/pdbe/pisa/). The results indicated that the interface between two β-sheets from two Amuc_1100 molecules is not the dimer interface but is a crystal-packing interface. However, the dimer interfaces of PilN, PilO and EpsL are comprised of β-sheets and additional α-helices nearby (Figs. 3*d*–3*f*). Therefore, the absence of a strong interaction between the corresponding helices provides additional evidence to support the monomeric state of Amuc_1100*.

4. Discussion

Previous studies of *A. muciniphila* have mainly focused on its role in glucose homeostasis and gut diseases (Zhao *et al.*,

2017). The proteins on the bacterial surface that directly interact with human intestinal cells are worth researching. A previous study suggested that Amuc_1100 was an outer membrane protein (Ottman *et al.*, 2017). Along with two other members, Amuc_1099 and Amuc_1101, Amuc_1100 is located within the gene cluster involved in type IV pilus-like formation (Ottman *et al.*, 2017). Thus, Amuc_1100 was defined as a pilus-like protein. The structural similarity between Amuc_1100 and PilO, PilN and EpsL indicates their functional similarity in pilus formation. Based on studies of T4P formation, PilN and PilO are critical for T4P biogenesis (Berry & Pelicic, 2015). The residues located in the N-terminus of PilN from *Neisseria meningitidis* are important for its function, especially residues Asn8 and Leu9 (Georgiadou *et al.*, 2012). The architecture of the T4P pilus machine from *Myxococcus xanthus* revealed that PilO is located in the lower periplasmic ring (Chang *et al.*, 2016), and *pilO* knockout disrupted T4P formation (Friedrich *et al.*, 2014). The knockout of other genes involved in the PilMNOPQ subcomplex also abolished T4P biogenesis (Friedrich *et al.*, 2014). Furthermore, three generated covalent pairs ($PilN^{R142C}$/$PilO^{D175C}$, $PilO^{A158C}$/$PilO^{I178C}$ and $PilO^{Y154C}$/$PilO^{I178C}$) caused a significant loss of surface piliation (Leighton *et al.*, 2016). Therefore, the interaction between Amuc_1100 and its related proteins should be further examined.

Interestingly, studies of pilus biogenesis showed that PilN and PilO are located in the inner membrane of the bacterium (Sampaleanu *et al.*, 2009; Rumszauer *et al.*, 2006; Ayers *et al.*, 2009) and EpsL is also a bitopic inner membrane T2SS protein (Abendroth *et al.*, 2009), whereas Amuc_1100 is an outer membrane protein (Ottman *et al.*, 2017). The different locations of these proteins might be associated with their features.

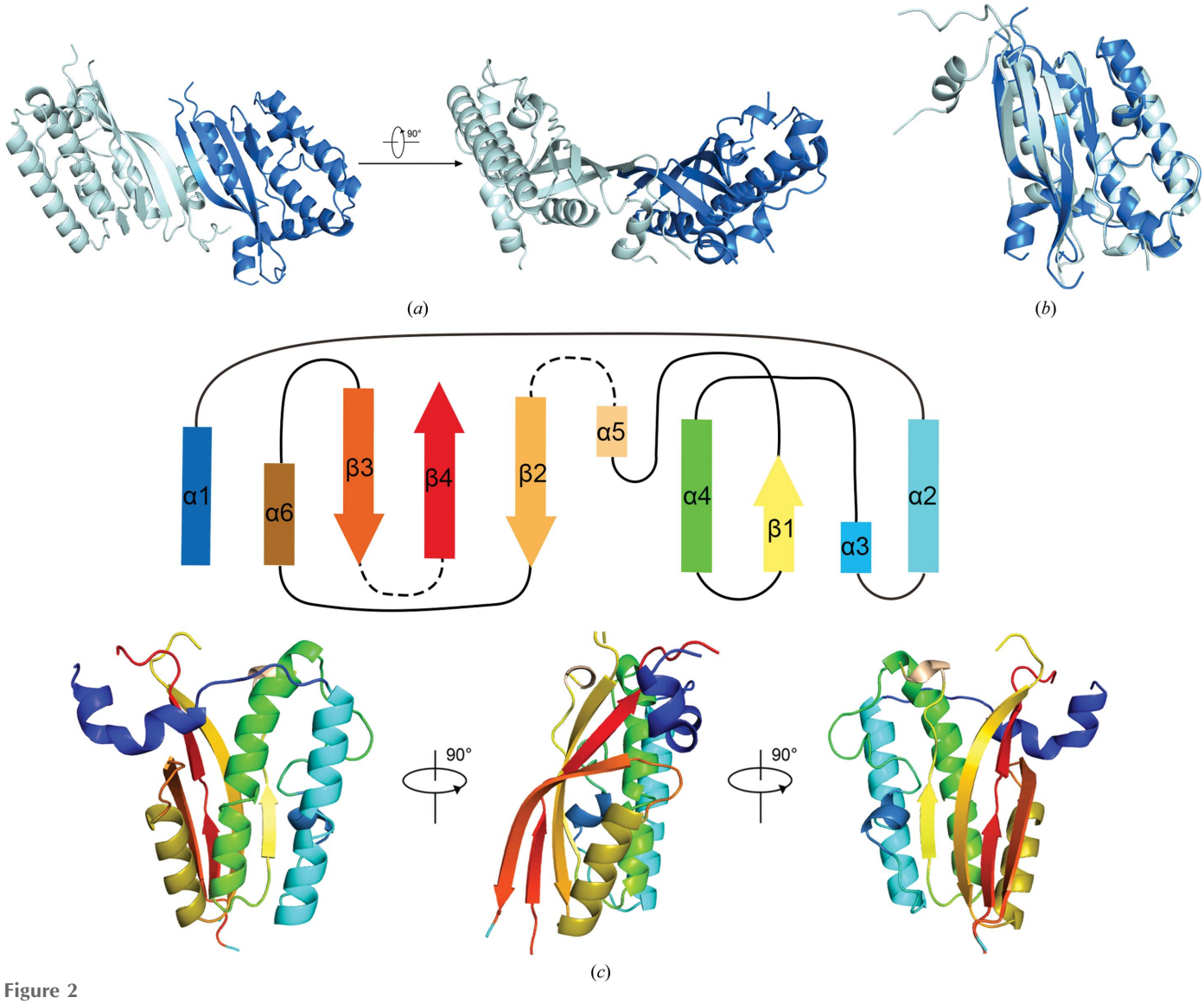

Figure 2
Crystal structure of Amuc_1100*. (*a*) Overall structure of Amuc_1100*. The proteins pack as dimers in the crystal lattice. The two protomers are colored pale cyan and marine blue. (*b*) Alignment of the two protomers of Amuc_1100* (r.m.s.d. = 0.4 Å). (*c*) General topology of Amuc_1100*; rectangles represent α-helices and arrows represent β-sheets. The dashed lines represent absent fragments. The lower panel shows the struucture of the Amuc_1100* monomer in the corresponding colors. All structure-related figures were prepared in *PyMOL* (Schrödinger).

Their different oligomeric states also indicate distinct functions. Furthermore, there are 15 highly conserved proteins related to piliation (Berry & Pelicic, 2015). Amuc_1100, however, shares low sequence similarity with them. Notably, Amuc_1101, which was identified as a cell-division protein named FtsA, has a sequence identity of 99% with PilM from *E. coli*, indicating that Amuc_1099 and Amuc_1100 might be involved in pilus formation. In short, the functional details of Amuc_1100 need to be further elucidated, in particular its function in pili formation.

In the dimeric structures of PilO and PilN the N-terminal coiled-coil domains mediate dimerization, which is consistent with previous functional identification of the coiled-coil domain (Sampaleanu *et al.*, 2009; Mason & Arndt, 2004). Interestingly, Amuc_1100 also has a predicted coiled-coil domain (residues 65–85). Notably, the predicted coiled-coil domain was only partially included in our structure because of trypsin cleavage. However, in biochemical assays, even with the complete predicted coiled-coil domain Amuc_1100* does not form a dimer. The results indicated that the predicted coiled-coil domain in Amuc_1100* may not be involved in mediating dimerization or, more likely, dimerization is a joint result of both the predicted coiled-coil domain and additional factor(s) on the surface of *A. muciniphila* or recipient cells. This potential property of Amuc_1100 needs further investigation.

More recently, studies of *A. muciniphila* have found that this intestinal bacterium has various effects on human diseases, particularly gut diseases (Png *et al.*, 2010). *A. muciniphila* is a potential candidate for therapeutic

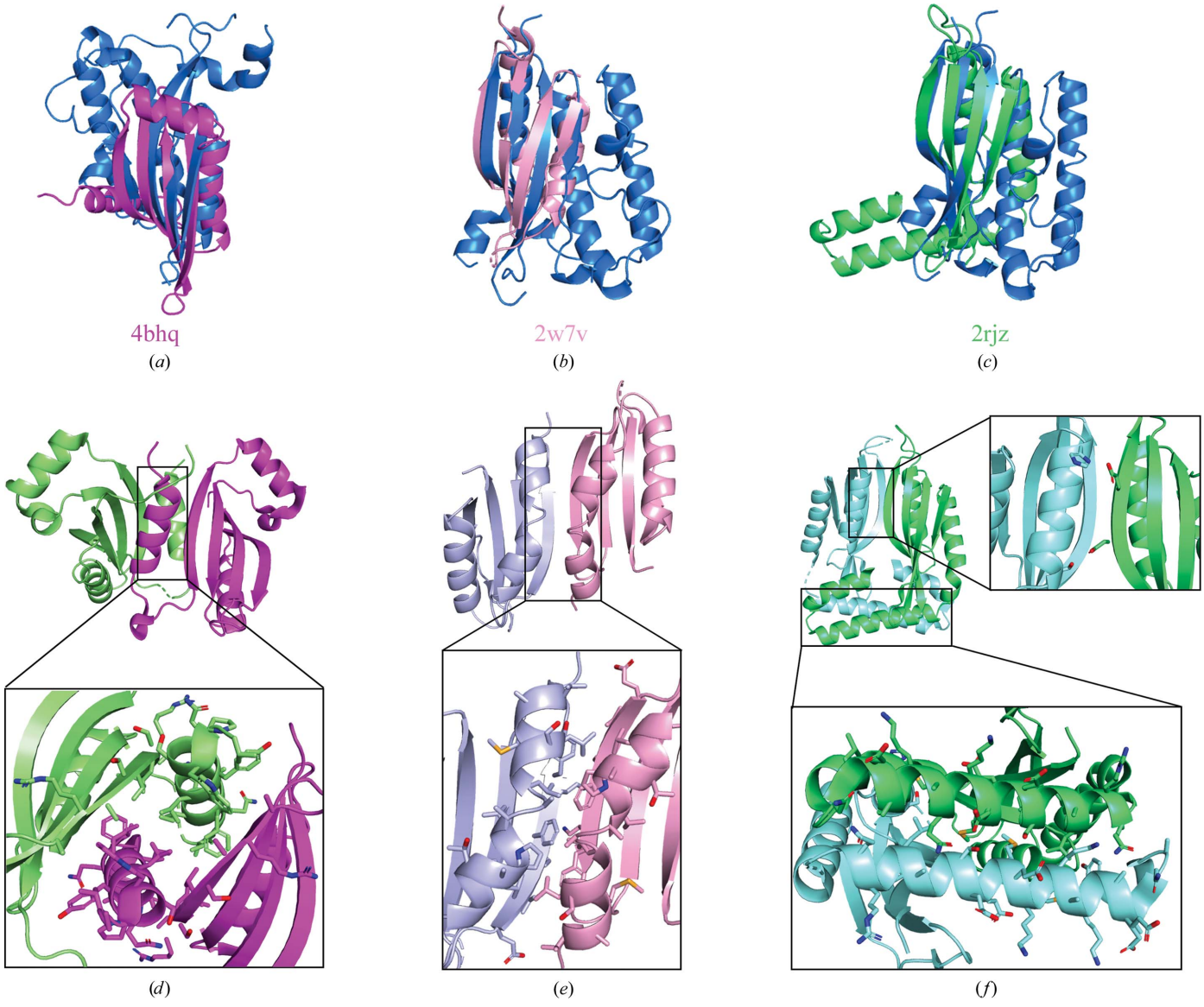

Figure 3
Alignment of Amuc_1100* with structurally similar proteins. (*a*, *b*, *c*) Structural comparison of chain *A* (marine blue) of Amuc_1100* and PilN (PDB entry 4bhq; magenta; Karuppiah *et al.*, 2013), EpsL (PDB entry 2w7v; pink; Abendroth *et al.*, 2009) and PilO (PDB entry 2rjz; green; Sampaleanu *et al.*, 2009). The alignment targets were selected from the *DALI* results for Amuc_1100*. (*d*, *e*, *f*) Dimeric interfaces in the structures of PilN (*d*), EpsL (*e*) and PilO (*f*).

medication, and its outer membrane structure may be involved in its interaction with intestinal tissues. Thus, more attention should be given to the components of its outer membrane. Structural investigation of Amuc_1100 will not only facilitate the understanding of the therapeutic mechanism of *A. muciniphila* but will also shed light on the formation of T4P in *A. muciniphila.*

Acknowledgements

We thank the staff of beamline BL19U1 at Shanghai Synchrotron Radiation Facility for on-site assistance.

Funding information

Funding for this research was provided by: Sichuan Youth Science and Technology Foundation (grant No. 2017JQ0007).

References

Abendroth, J., Kreger, A. C. & Hol, W. G. J. (2009). *J. Struct. Biol.* **168**, 313–322.

Ayers, M., Sampaleanu, L. M., Tammam, S., Koo, J., Harvey, H., Howell, P. L. & Burrows, L. L. (2009). *J. Mol. Biol.* **394**, 128–142.

Bahar, O., Goffer, T. & Burdman, S. (2009). *Mol. Plant Microbe Interact.* **22**, 909–920.

Berry, J. L. & Pelicic, V. (2015). *FEMS Microbiol. Rev.* **39**, 134–154.

Cani, P. D. & de Vos, W. M. (2017). *Front. Microbiol.* **8**, 1765.

Chang, Y.-W., Rettberg, L. A., Treuner-Lange, A., Iwasa, J., Sogaard-Andersen, L. & Jensen, G. J. (2016). *Science*, **351**, aad2001.

Clemente, J. C., Ursell, L. K., Parfrey, L. W. & Knight, R. (2012). *Cell*, **148**, 1258–1270.

Collado, M. C., Derrien, M., Isolauri, E., de Vos, W. M. & Salminen, S. (2007). *Appl. Environ. Microbiol.* **73**, 7767–7770.

Craig, L., Pique, M. E. & Tainer, J. A. (2004). *Nat. Rev. Microbiol.* **2**, 363–378.

Dao, M. C., Everard, A., Aron-Wisnewsky, J., Sokolovska, N., Prifti, E., Verger, E. O., Kayser, B. D., Levenez, F., Chilloux, J., Hoyles, L., MICRO-Obes Consortium, Dumas, M. E., Rizkalla, S. W., Doré, J., Cani, P. D. & Clément, K. (2016). *Gut*, **65**, 426–436.

Derrien, M., Collado, M. C., Ben-Amor, K., Salminen, S. & de Vos, W. M. (2008). *Appl. Environ. Microbiol.* **74**, 1646–1648.

Derrien, M., Vaughan, E. E., Plugge, C. M. & de Vos, W. M. (2004). *Int. J. Syst. Evol. Microbiol.* **54**, 1469–1476.

Emsley, P., Lohkamp, B., Scott, W. G. & Cowtan, K. (2010). *Acta Cryst.* D**66**, 486–501.

Everard, A., Belzer, C., Geurts, L., Ouwerkerk, J. P., Druart, C., Bindels, L. B., Guiot, Y., Derrien, M., Muccioli, G. G., Delzenne, N. M., de Vos, W. M. & Cani, P. D. (2013). *Proc. Natl Acad. Sci. USA*, **110**, 9066–9071.

Friedrich, C., Bulyha, I. & Søgaard-Andersen, L. (2014). *J. Bacteriol.* **196**, 378–390.

Georgiadou, M., Castagnini, M., Karimova, G., Ladant, D. & Pelicic, V. (2012). *Mol. Microbiol.* **84**, 857–873.

Holm, L. & Sander, C. (1995). *Trends Biochem. Sci.* **20**, 478–480.

Karuppiah, V., Collins, R. F., Thistlethwaite, A., Gao, Y. & Derrick, J. P. (2013). *Proc. Natl Acad. Sci. USA*, **110**, E4638–E4647.

Leighton, T. L., Yong, D. H., Howell, P. L. & Burrows, L. L. (2016). *J. Biol. Chem.* **291**, 19923–19938.

Li, J., Lin, S., Vanhoutte, P. M., Woo, C. W. & Xu, A. (2016). *Circulation*, **133**, 2434–2446.

Li, Y., Innocentin, S., Withers, D. R., Roberts, N. A., Gallagher, A. R., Grigorieva, E. F., Wilhelm, C. & Veldhoen, M. (2011). *Cell*, **147**, 629–640.

Liebschner, D., Afonine, P. V., Baker, M. L., Bunkóczi, G., Chen, V. B., Croll, T. I., Hintze, B., Hung, L.-W., Jain, S., McCoy, A. J., Moriarty, N. W., Oeffner, R. D., Poon, B. K., Prisant, M. G., Read, R. J., Richardson, J. S., Richardson, D. C., Sammito, M. D., Sobolev, O. V., Stockwell, D. H., Terwilliger, T. C., Urzhumtsev, A. G., Videau, L. L., Williams, C. J. & Adams, P. D. (2019). *Acta Cryst.* D**75**, 861–877.

Mason, J. M. & Arndt, K. M. (2004). *ChemBioChem*, **5**, 170–176.

McCoy, A. J., Grosse-Kunstleve, R. W., Adams, P. D., Winn, M. D., Storoni, L. C. & Read, R. J. (2007). *J. Appl. Cryst.* **40**, 658–674.

Minor, W., Cymborowski, M., Otwinowski, Z. & Chruszcz, M. (2006). *Acta Cryst.* D**62**, 859–866.

Ottman, N., Huuskonen, L., Reunanen, J., Boeren, S., Klievink, J., Smidt, H., Belzer, C. & de Vos, W. M. (2016). *Front. Microbiol.* **7**, 1157.

Ottman, N., Reunanen, J., Meijerink, M., Pietilä, T. E., Kainulainen, V., Klievink, J., Huuskonen, L., Aalvink, S., Skurnik, M., Boeren, S., Satokari, R., Mercenier, A., Palva, A., Smidt, H., de Vos, W. M. & Belzer, C. (2017). *PLoS One*, **12**, e0173004.

Plovier, H., Everard, A., Druart, C., Depommier, C., Van Hul, M., Geurts, L., Chilloux, J., Ottman, N., Duparc, T., Lichtenstein, L., Myridakis, A., Delzenne, N. M., Klievink, J., Bhattacharjee, A., van der Ark, K. C., Aalvink, S., Martinez, L. O., Dumas, M. E., Maiter, D., Loumaye, A., Hermans, M. P., Thissen, J. P., Belzer, C., de Vos, W. M. & Cani, P. D. (2017). *Nat. Med.* **23**, 107–113.

Png, C. W., Lindén, S. K., Gilshenan, K. S., Zoetendal, E. G., McSweeney, C. S., Sly, L. I., McGuckin, M. A. & Florin, T. H. (2010). *Am. J. Gastroenterol.* **105**, 2420–2428.

Reunanen, J., Kainulainen, V., Huuskonen, L., Ottman, N., Belzer, C., Huhtinen, H., de Vos, W. M. & Satokari, R. (2015). *Appl. Environ. Microbiol.* **81**, 3655–3662.

Rice, L. M., Earnest, T. N. & Brunger, A. T. (2000). *Acta Cryst.* D**56**, 1413–1420.

Rumszauer, J., Schwarzenlander, C. & Averhoff, B. (2006). *FEBS J.* **273**, 3261–3272.

Sampaleanu, L. M., Bonanno, J. B., Ayers, M., Koo, J., Tammam, S., Burley, S. K., Almo, S. C., Burrows, L. L. & Howell, P. L. (2009). *J. Mol. Biol.* **394**, 143–159.

Shen, W., Shen, M., Zhao, X., Zhu, H., Yang, Y., Lu, S., Tan, Y., Li, G., Li, M., Wang, J., Hu, F. & Le, S. (2017). *Front. Microbiol.* **8**, 272.

Vigsnaes, L. K., Brynskov, J., Steenholdt, C., Wilcks, A. & Licht, T. R. (2012). *Benef. Microbes*, **3**, 287–297.

Winn, M. D., Ballard, C. C., Cowtan, K. D., Dodson, E. J., Emsley, P., Evans, P. R., Keegan, R. M., Krissinel, E. B., Leslie, A. G. W., McCoy, A., McNicholas, S. J., Murshudov, G. N., Pannu, N. S., Potterton, E. A., Powell, H. R., Read, R. J., Vagin, A. & Wilson, K. S. (2011). *Acta Cryst.* D**67**, 235–242.

Zhao, S., Liu, W., Wang, J., Shi, J., Sun, Y., Wang, W., Ning, G., Liu, R. & Hong, J. (2017). *J. Mol. Endocrinol.* **58**, 1–14.